Electronic Supplementary Material (ESI) for Chemical Communications.

A smart approach to achieve exceptionally high loading of metal nanoparticles supported by functionalized extended frameworks for efficient catalysis

Bappaditya Gole, Udishnu Sanyal & Partha Sarathi Mukherjee*

Department of Inorganic and Physical Chemistry, Indian Institute of Science

Bangalore 560012, India

Supporting Information

Contents:

1. Experimental section

1.1. Materials and methods

All the chemicals/solvents were obtained from different commercial sources and used without further purification, unless otherwise mentioned. 5-(prop-2-yn-1-yloxy) isophthalic acid (*pip*) and 1,4-di(pyridin-4-yl)benzene (*dpb*) were prepared according to the literature procedures.[1] NMR spectra were recorded using a Bruker 400 MHz spectrometer. The chemical shifts (δ) in the ^{1}H NMR spectra are reported in ppm relative to tetramethylsilane (TMS) as an internal standard (0.0 ppm). IR spectra were recorded on a Bruker ALPHA FT-IR spectrometer used in the range of 4000–400 cm^{-1}. Powder X-ray diffraction (PXRD) patterns were recorded on a Phillips PANalytical diffractometer for Cu Kα radiation (λ = 1.5406 Å), with a scan speed of 1° min^{-1}. Thermogravimetric (TGA) analyses of the MOFs were carried out on a *Metler-Toledo* thermal gravimetric analyzer under nitrogen flow. Electronic absorption spectral measurements were done using Perkin Elmer LAMBDA 750 UV/visible spectrophotometer. ESI-HRMS measurements were performed on an Agilent 6538 UHD accurate-mass Q-TOF LC/MS instrument. Inductively coupled plasma analyses (ICP) was performed on a Shimadzu ICPS-8100 equipment. Field emission scanning electron microscopy (FESEM) was carried out using Carl-Zeiss Ultra 55 microscope equipped with energy dispersive X-ray analysis (EDAX) at an operating voltage of 5-20 kV. EDAX analysis was carried out to determine the elemental composition of the samples. Samples for SEM were prepared by drop-casting the dispersion of samples in methanol onto pre-cleaned carbon tape. The TEM bright field (BF) images, selected area electron diffraction (SAED) patterns, high resolution TEM (HRTEM) images, and the high-angle annular dark field (HAADF) images were acquired using a JEOL 2100F field emission transmission electron microscope, operating at 200 kV. To prepare the TEM samples, the Au@MOFs were first re-dispersed in methanol by sonication for about 15 min and then the solution was placed on a carbon coated copper grid and finally dried under a lamp.

1.2. Synthesis and general characterizations

Synthesis of MOF-1: $Zn(NO_3)_2{\cdot}6H_2O$ (2.9 mg, 0.01 mmol), *H_2pip* (2.2 mg, 0.01 mmol) and 4,4′-bipyridine (1.6 mg, 0.01 mmol) were taken in an 8 mL scintillation vial. 3 mL dimethylformamide (DMF) was then added. The vial was stirred for 10 min to get a clear solution. The reaction vial was capped and then placed in a programmable oven and heated at 90 °C for 2 days and cooled to room temperature at the rate of 0.15°C/min. Colorless needle shaped crystals (1.8 mg, 60%) of the

product were collected by filtration and washed with DMF (3 × 5 mL). IR spectra (υ/cm^{-1}): 3270, 3074, 1973, 1612, 1554, 1450, 1375, 1317, 1127, 1044, 937, 908, 780, 722, 675, 632.

Synthesis of MOF-2: $Zn(NO_3)_2{\cdot}6H_2O$ (3 mg, 0.01 mmol), *H_2pip* (2.2 mg, 0.01 mmol) and 1,2-bis(pyridin-4-yl)ethane (bpe) (1.8 mg, 0.01 mmol) were taken in an 8 mL scintillation vial. Subsequently 3 mL dimethylformamide (DMF) was added. The vial was stirred for 10 min to dissolve all the components. The reaction vial was capped and then placed in a programmable oven and heated at 90 °C for 2 days and cooled at a rate of 0.15°C/min. Colorless crystals (2.5 mg, 67%) of the product were collected by filtration and washed with DMF (3 × 5 mL). IR spectra (υ/cm^{-1}) 3194, 1997, 1615, 1560, 1409, 1351, 1266, 1230, 1125, 1038, 934, 904, 815, 776, 722, 679, 523.

Synthesis of MOF-3: $Zn(NO_3)_2{\cdot}6H_2O$ (3 mg, 0.01 mmol), *H_2pip* (2.2 mg, 0.01 mmol) and 1,4-di(pyridin-4-yl)benzene (dpb) (2.3 mg, 0.01 mmol) were taken in a 8 mL scintillation vial. To that 3 mL dimethylformamide (DMF) was added. The vial was stirred for 10 min at room temperature to dissolve all the components. The reaction vial was capped and placed in a programmable oven and heated at 90 °C for 2 days and cooled at the rate of 0.15 °C/min. Colorless needle shape crystals (2.0 mg, 62%) of the product were collected by filtration and subsequently washed with DMF (3 × 5 mL). IR spectra (υ/cm^{-1}): 3223, 1660, 1613, 1559, 1488, 1448, 1374, 1249, 1130, 1094, 1042, 936, 906, 809, 780, 719, 660, 548, 488, 443.

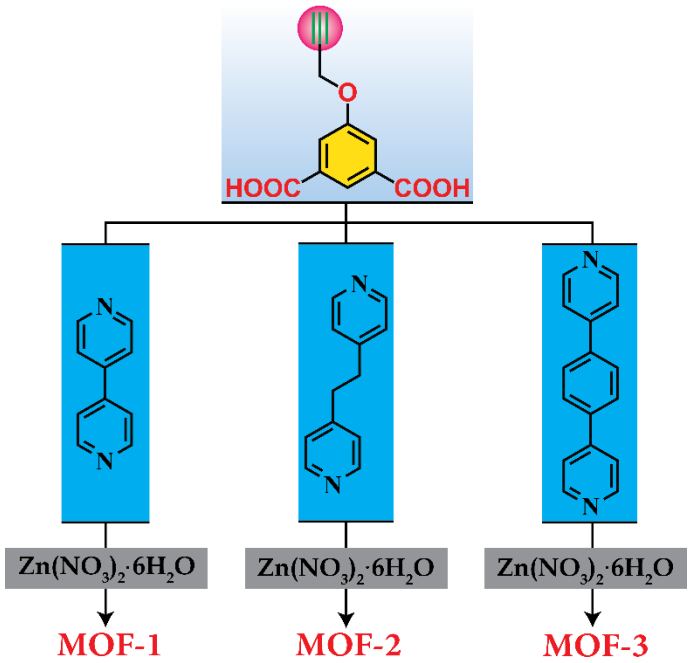

Scheme S1. Schematic representation of preparation of different MOFs depending of the pillar height of the bipyridyl linkers.

Synthesis of MOF-A: **MOF-A** was prepared according to the earlier procedure for control experiments.[2] $Zn(NO_3)_2 \cdot 6H_2O$ (6 mg, 0.02 mmol), 5-(benzyloxy)isophthalic acid (5.5 mg, 0.02 mmol) and 1,4-di(pyridin-4-yl)benzene (dpb) (4.6 mg, 0.02 mmol) were taken in a 8 mL scintillation vial. To that 3 mL DMF was added and the mixture was stirred for 10 min at room temperature to get a clear solution. The reaction vial was capped tightly and placed in a programmable oven and heated at 120 °C for 24 h followed by slow cooling to room temperature at a cooling rate of 15 °C/h. Colorless crystals of the product were collected by filtration and washed with fresh DMF (2 × 3 mL). Phase purity of the as synthesized **MOF-A** was established by comparing PXRD with earlier report.

Table S1. Crystallographic parameters of the **MOF-1** and **MOF-2**. (CCDC No. 1029507 and 1029508 respectively)

	MOF-1	***MOF-2***
Empirical formula	$C_{21}H_{14}O_5N_2Zn$	$C_{23}H_{18}O_5N_2Zn$
FW	439.73	467.78
T (K)	90(2)	90(2)
Crystal system	Monoclinic	Monoclinic
Space group	$P2_1/c$	*C2/c*
a/Å	11.361(5)	29.971(8)
b/Å	15.532(5)	16.271(4)
c/Å	16.269(5)	15.804(4)
α/deg	90	90
β/deg	94.66(5)	115.749(7)
γ/deg	90	90
V/Å^3	2861.3(18)	6942(3)
Z	4	8
ρ_{calcd} (g cm^{-3})	1.383	0.887
μ(Mo Kα) (mm^{-1})	0.912	0.730
λ/Å	0.71073	0.71073
F (000)	1224.0	1888.0
Collected reflns	5765	7100
Unique reflns	4620	4780
GOF *(F^2)*	0.909	1.215
R_1[a]	0.0607	0.1051
wR_2[b]	0.1913	0.3192

[a] $R_1 = \Sigma \left| F_o - F_c \right| / \Sigma \left| F_o \right|$; [b] $wR_2 = \Sigma[w(F_o^2 - F_c^2)^2] / w(F_o^2)^2]^{1/2}$

1.3. Activation of MOFs

All the as-synthesized crystalline MOFs (about 150 mg) were soaked in methanol and the supernatant methanol was discarded in every 8 h (3 times) and fresh methanol was added subsequently each time. After methanol exchange, the sample was treated further in the same way with acetone and dichloromethane to remove methanol and acetone, respectively. Finally,

the dichloromethane was decanted and the sample was dried under a dynamic vacuum at 110 °C for 6 h.

1.4. Single crystal X-ray diffraction analysis

A Crystal of the corresponding MOF was coated with paratone oil and the diffraction data were collected at 90 K on a Bruker SMART APEX CCD diffractometer using SMART/SAINT software.[3] Intensity data were collected using graphite-monochromatized Mo-Kα radiation (0.71073 Å) at 90 K. The structure was solved by direct methods using the SHELX-97 program[4] incorporated into WinGX.[5] Empirical absorption corrections were applied with SADABS.[6] All non-hydrogen atoms were refined with anisotropic displacement coefficients. The hydrogen atoms linked to carbon were included in geometric positions and were given thermal parameters equivalent to 1.2 times those of the atom to which they were attached. The hydrogen atoms of the solvent water molecule were not included in the least-squares refinement. Structure refinement after modification of the data for the solvent molecules with the SQUEEZE routine of PLATON led to better refinement and data convergence. Though the as synthesized **MOF-3** was obtained in highly crystalline form, several attempts remained unsuccessful to obtain diffraction quality single crystals for structure determination. Nevertheless, an analogous structural arrangement similar to **MOF-1** and **MOF-2** has been confirmed by PXRD pattern. The crystallographic refinement parameters are given in Table S1. The crystallographic files are deposited on CCDC (CCDC No. 1029507 and 1029508 for **MOF-1** and **MOF-2** respectively).

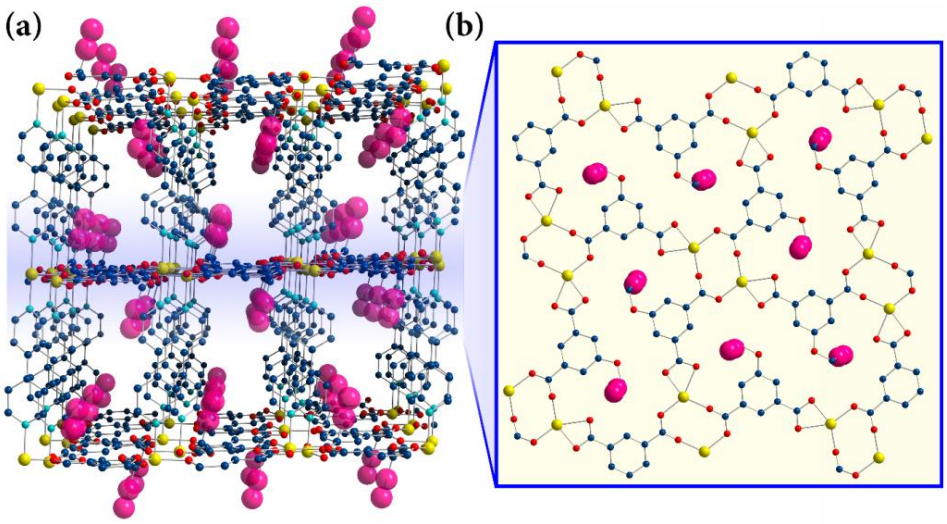

Fig. S1. *Crystal structure of* ***MOF-1****. (a) Extended three-dimensional network of* ***MOF-1*** *showing channel like pores. Each pore is decorated by functionalized alkyne moieties. (b) Two-dimensional layered network involving iph units of pip and* Zn^{II} *ions. The alkyne moieties are highlighted in pink color. Color codes: yellow, cyan, navy blue and red represent Zn, N, C and O respectively.*

1.5. Synthesis of metal nanoparticles@MOFs

Activated MOFs were used for the preparation of MOF supported MNPs. Wet chemical method was employed to generate MNPs. In case of **MOF-3**, MNPs loading amount was gradually increased starting from 5 wt % until it gets saturated. For others MOFs, a constant amount of MNP was loaded based on the result obtained in the case of **MOF-3**. The maximum loading amount was reproduced for bulk scale preparation.

5 wt % Au@MOF-3: 5 mg of activated **MOF-3** was taken in 4 mL of methanol. To that 0.43 mg (1.26×10^{-3} mmol) of $HAuCl_4$ in 1 mL of methanol was added slowly. The mixture was kept for stirring at room temperature for 30 min to adsorb Au^{3+} ions into the MOF. During this time the bright yellow color of the supernatant (due to $HAuCl_4$) became colorless and the MOF turned to yellow from colorless. Subsequently, 0.24 mg (6.3×10^{-3} mmol, 5 eqv.) of $NaBH_4$ was added with constant stirring for another 1 h. During this period, the mixture turned to dark purple indicating the formation of Au nanoparticles. Finally, the mixture was filtered and washed several times with fresh methanol. The solid material was then dried under vacuum.

20 wt % Au@MOF-3: This was prepared in a similar method as described above but instead 1.73 mg (5.1×10^{-3} mmol) of $HAuCl_4$ was added to 5 mg of MOF in methanol. Subsequently, 1 mg (2.54×10^{-2} mmol, 5 eqv.) of $NaBH_4$ was added for reduction of Au^{3+} ions.

50 wt % Au@MOF-3: This was also prepared in a similar method as described for 5 wt % loading but instead 4.31 mg (1.27×10^{-2} mmol) of $HAuCl_4$ was added in 5 mg of MOF in methanol. Subsequently, 2.4 mg (6.35×10^{-2} mmol, 5 eqv.) of $NaBH_4$ was added for the reduction of Au^{3+} ions.

50 wt % Au@MOF-1: This was prepared in a similar way as described above but **MOF-1** was used instead of **MOF-3**.

50 wt % Au@MOF-2: This was prepared in a similar way as described above but **MOF-2** was used instead of **MOF-3**.

1.6. Control experiments

5 wt % Au@MOF-A: To 5 mg of activated **MOF-A** in 4 mL of methanol, 0.43 mg (1.26×10^{-3} mmol) of $HAuCl_4$ in 1 mL of methanol was added slowly. The mixture was kept for stirring at room temperature for 30 min. Subsequently, 0.24 mg (6.3×10^{-3} mmol, 5 eqv.) of $NaBH_4$ was added with constant stirring for another 1 h. During this period, the mixture turned dark purple indicating the formation of Au nanoparticles. Finally, the mixture was filtered and washed several times with fresh methanol. The solid material was then dried under vacuum.

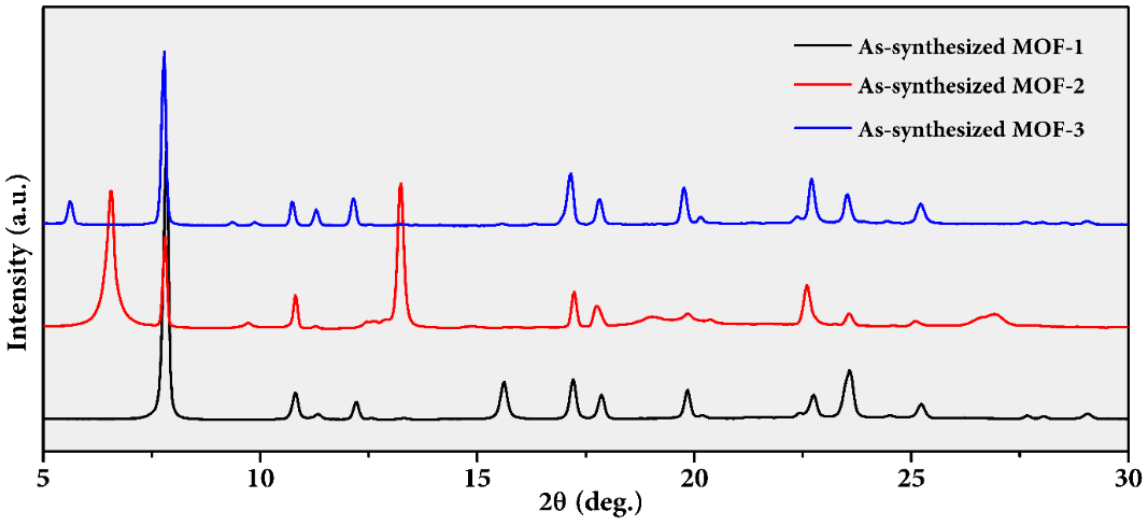

Fig. S2. *PXRD patterns of as-synthesized MOFs-**1**-**3**.*

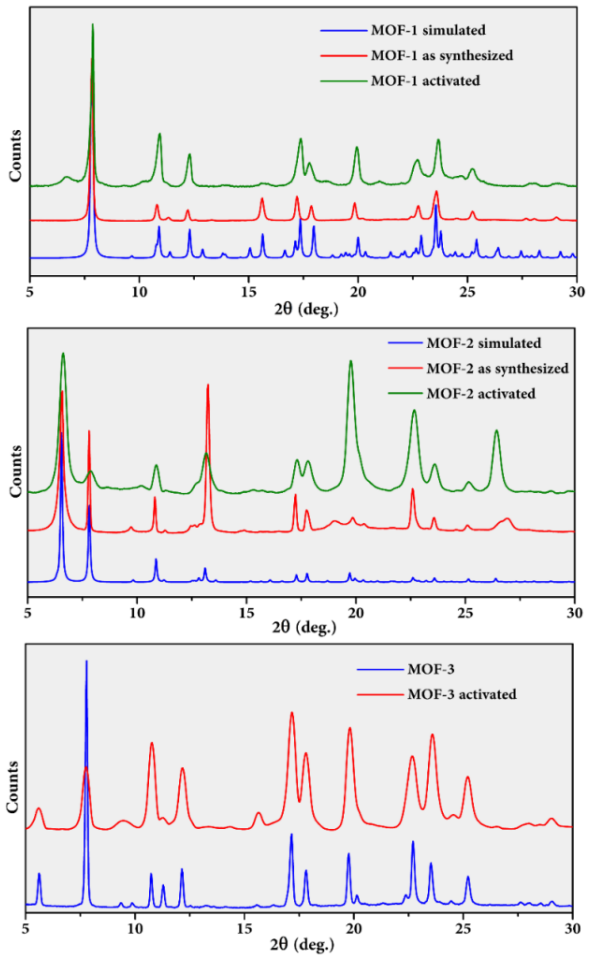

Fig. S3. *Comparison of simulated, as synthesized and activated PXRD patterns of different MOFs.*

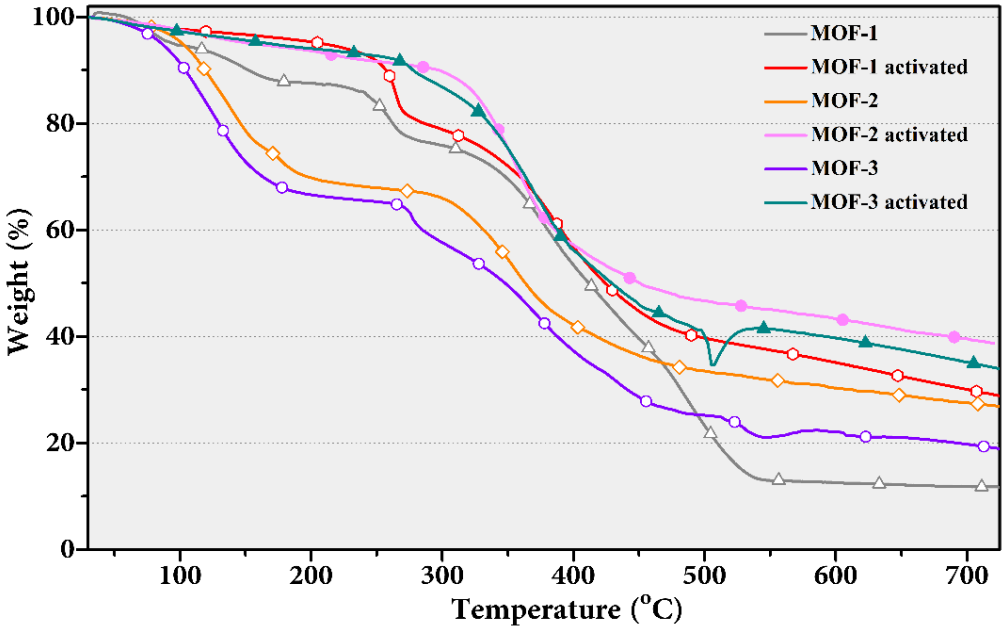

Fig. S4. *TGA plots of MOFs **1**-3 along with their activated forms.*

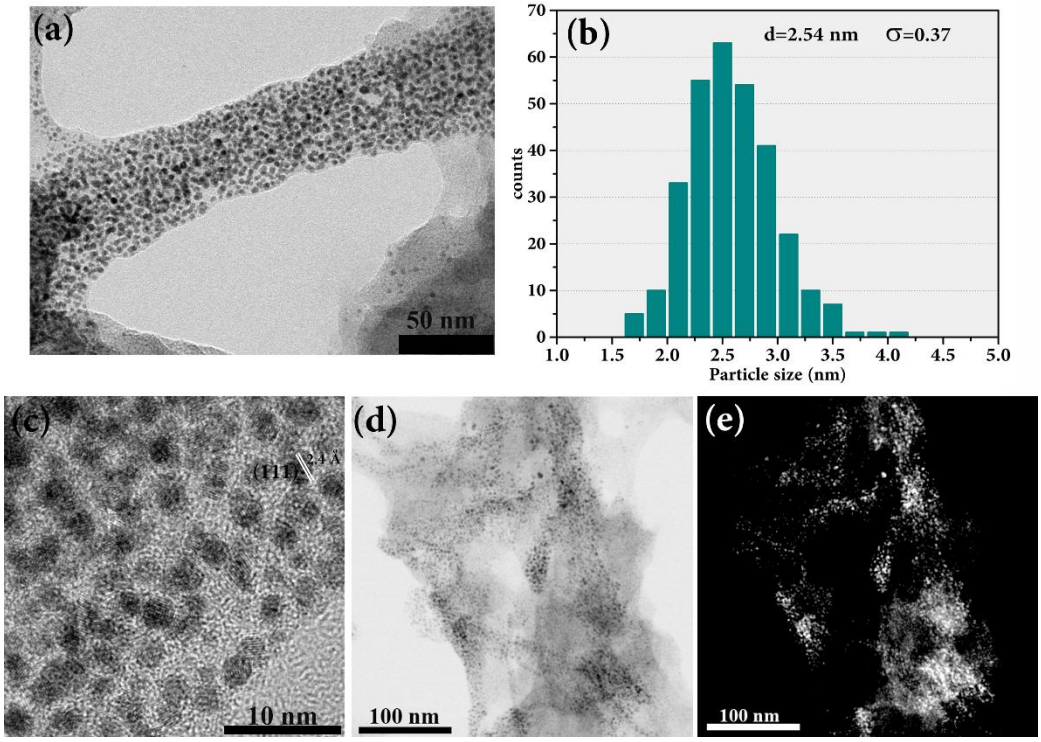

Fig. S5. 5 wt % Au loading in **MOF-3**. (a) Bright-field TEM image showing the Au NPs are homogeneously distributed in **MOF-3**. (b) Corresponding Au NPs size distribution histogram. (c) HRTEM image showing lattice spacing (d=2.4 A) corresponds to (111) plane of fcc Au. (d) STEM bright field image and (e) STEM-HAADF image of the **Au@MOF-3**.

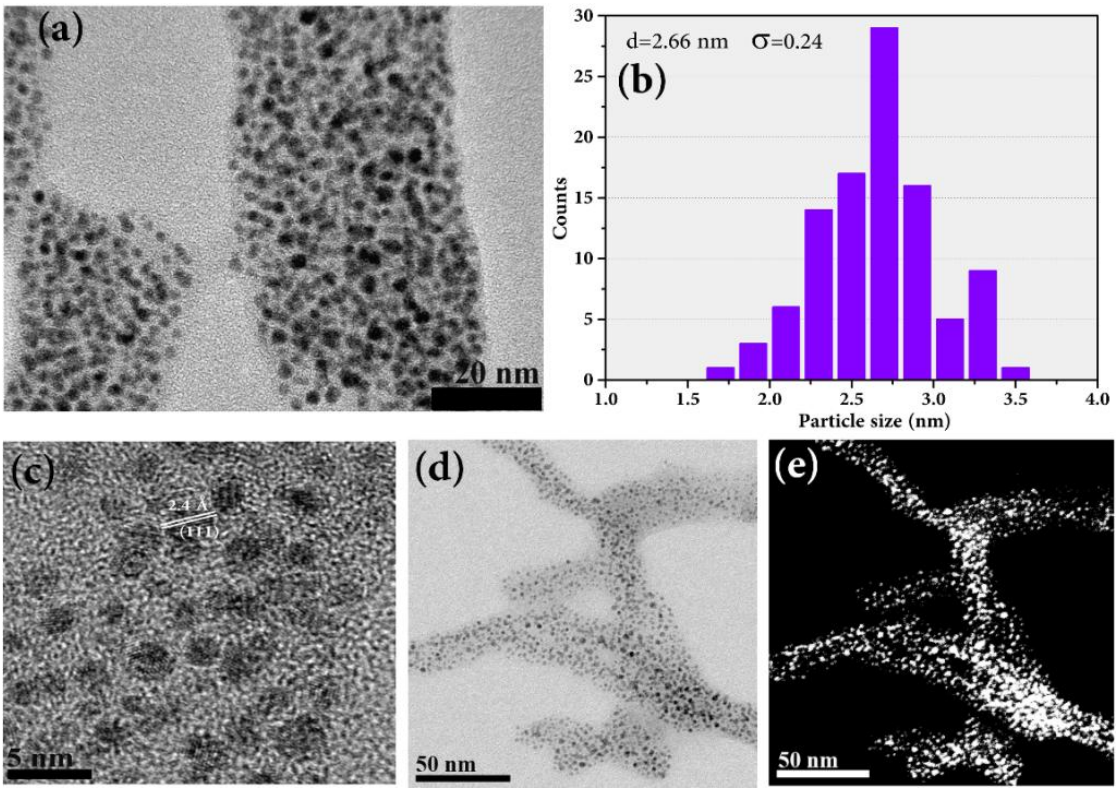

Fig. S6. *20 wt % Au loading in* ***MOF-3****. (a) Bright-field TEM image showing the Au NPs are homogeneously loaded in* ***MOF-3****. (b) Corresponding Au NPs size distribution histogram, (c) HRTEM image, (d) STEM bright field image and (e) STEM-HAADF image of the* ***Au@MOF-3*** *showing the Au particles as white spots.*

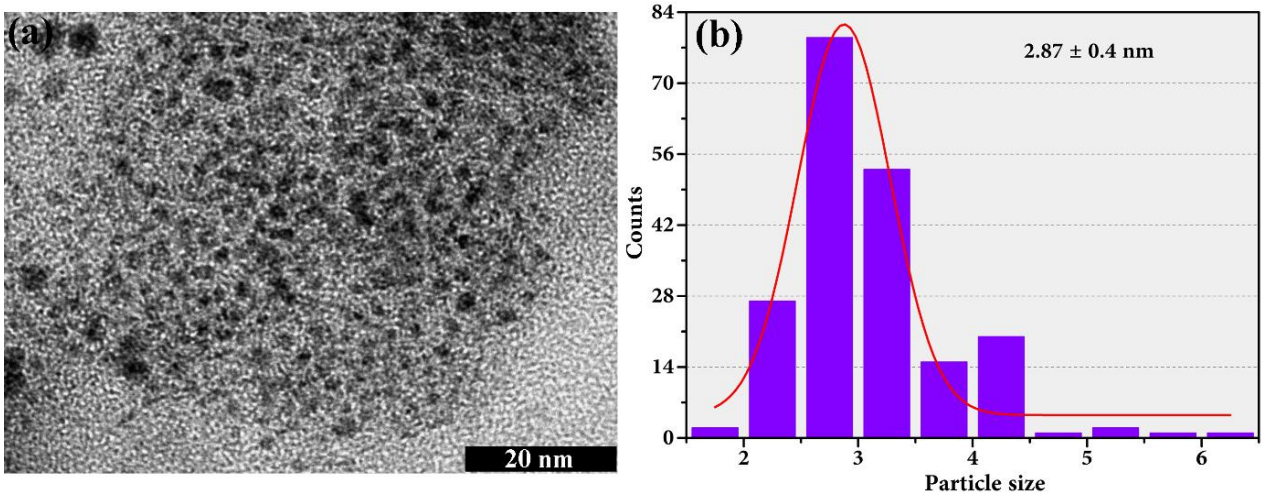

Fig. S7. *50 wt % loading of Au on* ***MOF-1****. (a) and (b) TEM-BF image of the Au NPs on* ***MOF-1*** *and corresponding size distribution respectively.*

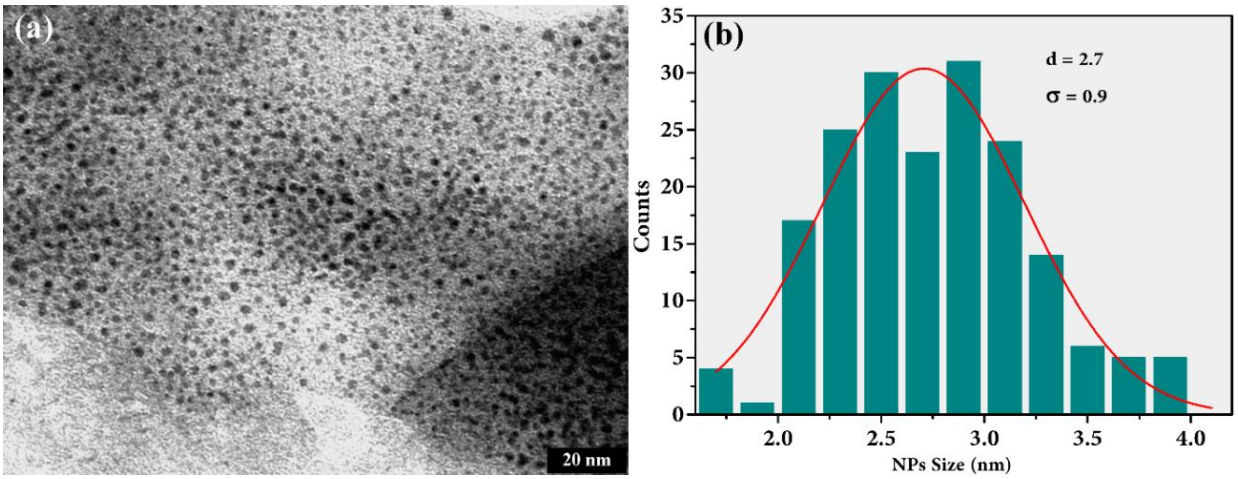

Fig. S8. *50 wt % loading of Au on* ***MOF-2****. (a) and (b) TEM-BF image of the Au NPs on* ***MOF-2*** *and corresponding size distribution respectively.*

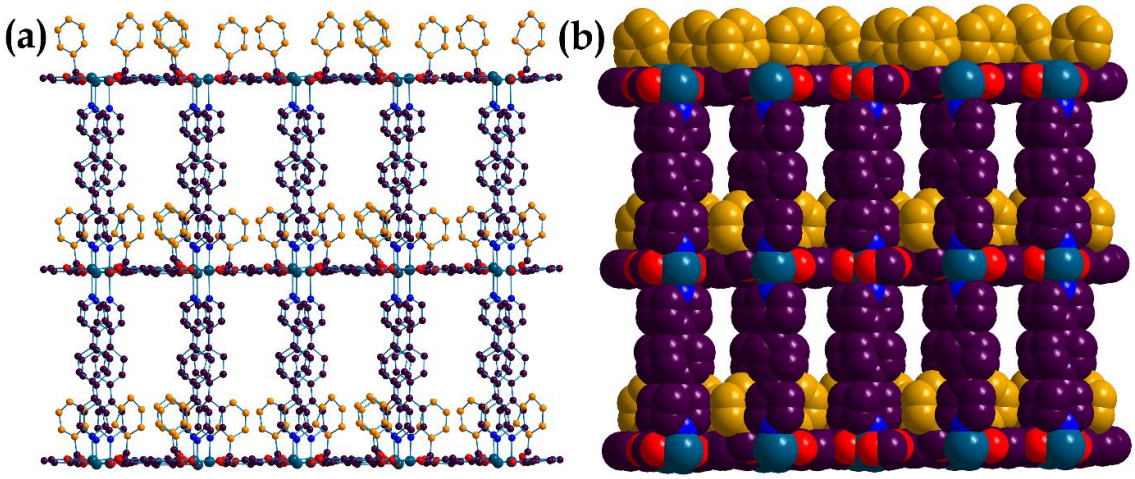

Fig. S9. *(a) Crystal structure of* ***MOF-A*** *and (b) corresponding space filling model indicated that the presence of phenyl moieties inside pore instead of alkyne functionality as observed in* ***MOFs-1*** *to* ***3****.*

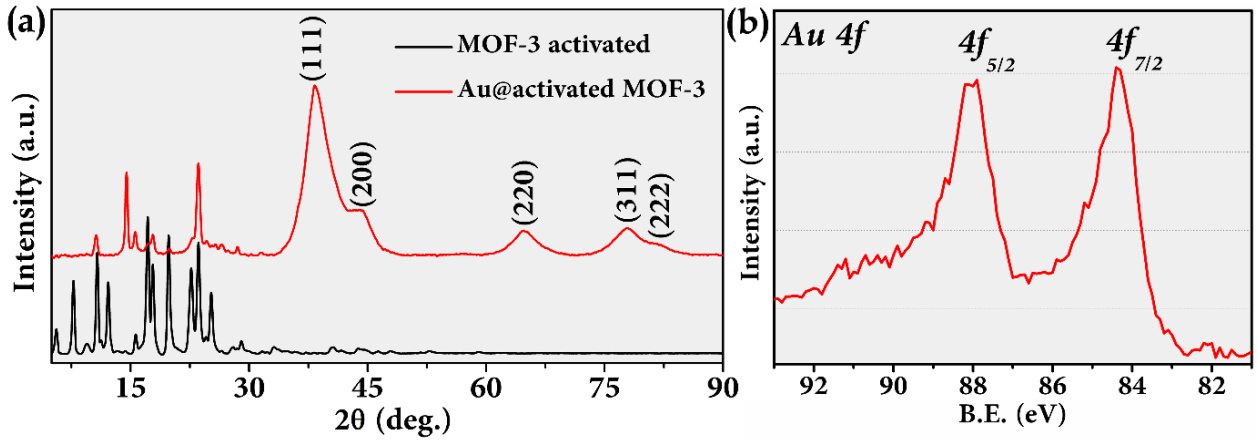

Fig. S10. (a) Comparison of PXRD patterns of activated MOF-3 and Au@MOF-3. (b) XPS spectrum of **Au@MOF-3**.

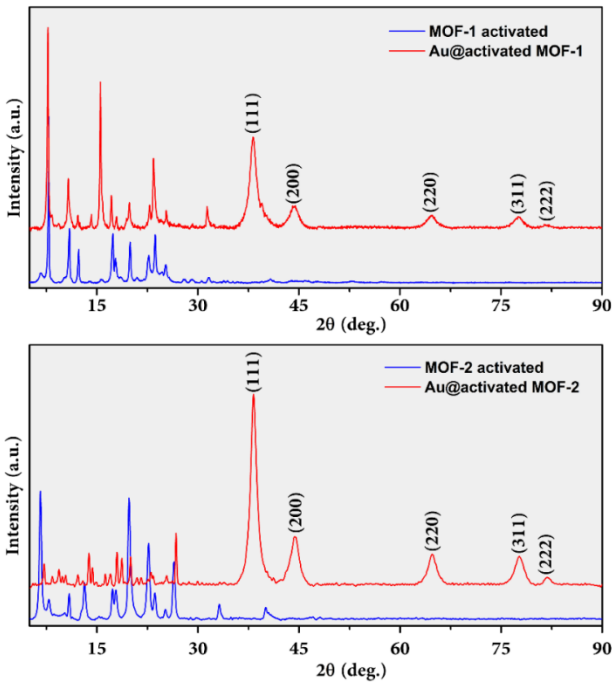

Fig. S11. *(a) Comparison of PXRD patterns of activated* ***MOF-1*** *and* ***MOF-2*** *with* ***Au@MOF-1*** *and* ***Au@MOF-2****, respectively.*

2. Comparison of IR spectra of MOF-3, $HAuCl_4$@MOF-3 and Au@MOF-3:

We checked the effect of $HAuCl_4$ and Au(0) loading on the band corresponds to alkyne stretching frequencies in IR spectrum of the **MOF-3**,. The weak band correspond to alkyne stretching in **MOF-3** at ~1950 cm^{-1} reduced significantly (**Fig. S12**) after loading of $HAuCl_4$ as well as after reduction to Au(0) which indicates that the ethynyl groups have distinct role in the stabilization of $HAuCl_4$ and Au(0) NPs.

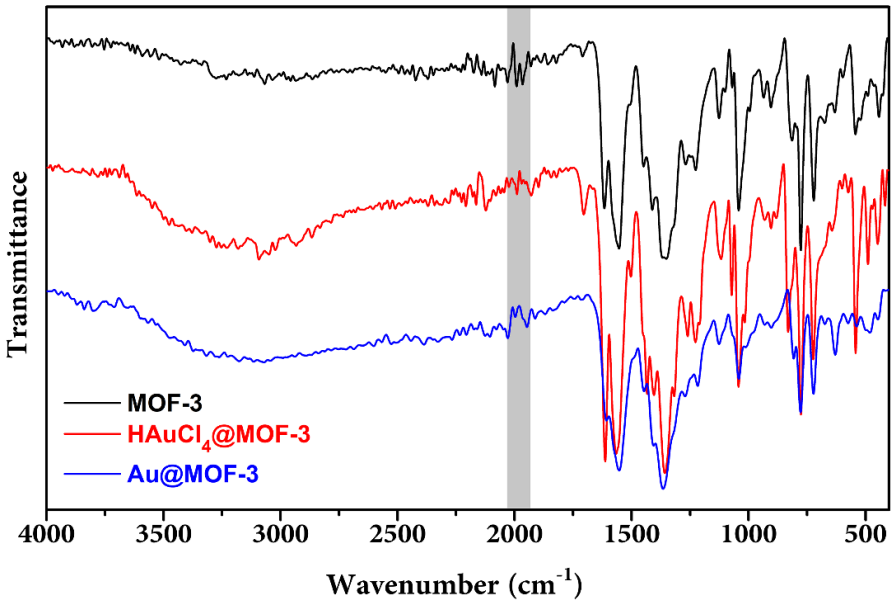

Fig. S12. IR spectra of **MOF-3**, **HAuCl4@MOF-3** and **Au@MOF-3**.

3. Au@MOFs catalyzed reduction of phenolic nitro compounds in water

In a typical reaction method, an aqueous stock solution of phenolic nitro compounds (50 mL, 0.2 mmol 4-nitrophenol and 2,4-dinitrophenol) and $NaBH_4$ (50 mL, 20 mmol) was prepared. The catalytic reduction was monitored by UV-vis absorption spectroscopy. Typically, 1 mL phenolic nitro compound and 1 mL $NaBH_4$ solution from stock were mixed together in a 3 mL quartz cuvette and subsequently the reduction process was monitored at room temperature by time drive absorbance measurement (in every 10 sec) at 400 nm and 360 nm for 4-NP and 2,4-DNP, respectively. The reduction process was monitored in a similar way in the presence of Au catalysts. After introducing the catalyst, the bright yellow solution of the reactants gradually faded with the progress of reaction. For Au induced catalytic process 5 mg of Au@MOFs and 0.002 mmol of $HAuCl_4$ were introduced. UV-vis spectra of the Au@MOFs catalytic reduction after 60 sec indicated complete disappearance of reactant peaks and appearance of new peak corresponds to reduced amino products. To study the reusability, the catalyst was filtered after the completion of the reaction. The catalyst was washed thoroughly with water and other organic solvents and subsequently dried under vacuum. The recovered catalyst was subsequently used for further catalytic cycles under identical condition.

Since the amount of $NaBH_4$ was used in much excess, the reduction of phenolic nitro compounds can be considered to follow pseudo first order kinetics. The corresponding rate is given below;

$$C_t = C_0 e^{-kt} \qquad (1)$$

Where, C_0 and C_t are initial concentration and concentration of phenolic nitro compounds at given time (t). k represents corresponding rate constant. If the reactants absorb light at a given wavelength and the products do not absorb in same wavelength, the absorbance can be used directly for determination of concentration of phenolic nitro compounds at a given time.

Since, $A_0 = \varepsilon l C_0$ and $A_t = \varepsilon l C_t$, where A_0 and A_t are initial and absorbance at different time (t). The ε and l are the molar extinction coefficient and path length, respectively. Then the equation (1) can be modified to

$$A_t = A_0 e^{-kt} \qquad (2)$$

Taking natural log on the both sides, equation (2) transforms to

$$ln(A_t) = ln(A_0) - kt \qquad (3)$$

Thus, the rate constant (k) can be estimated from $ln(A_t)$ vs t plot in the form of slope by linear fit using equation (3).

As expected, Figures S14(b) and S15(b) show typical linear relationship between $ln(A_t)$ vs t when only $NaBH_4$ and $NaBH_4$ + $HAuCl_4$ were used as reducing agents. However, $ln(A_t)$ vs t *plot* was deviated from linearity at higher time scale when **Au@MOFs** were used. Therefore, only initial part

was fitted to estimate the rate constants. The evaluated rate constants are provided in Table S2. Results clearly indicate that Au-NPs catalyzed reactions were extremely faster than the reaction with $NaBH_4$ or $NaBH_4$ + $HAuCl_4$. These values showed the superiority of the present **Au@MOFs** as catalysts compared to many other Au-based catalysts under similar reaction conditions.

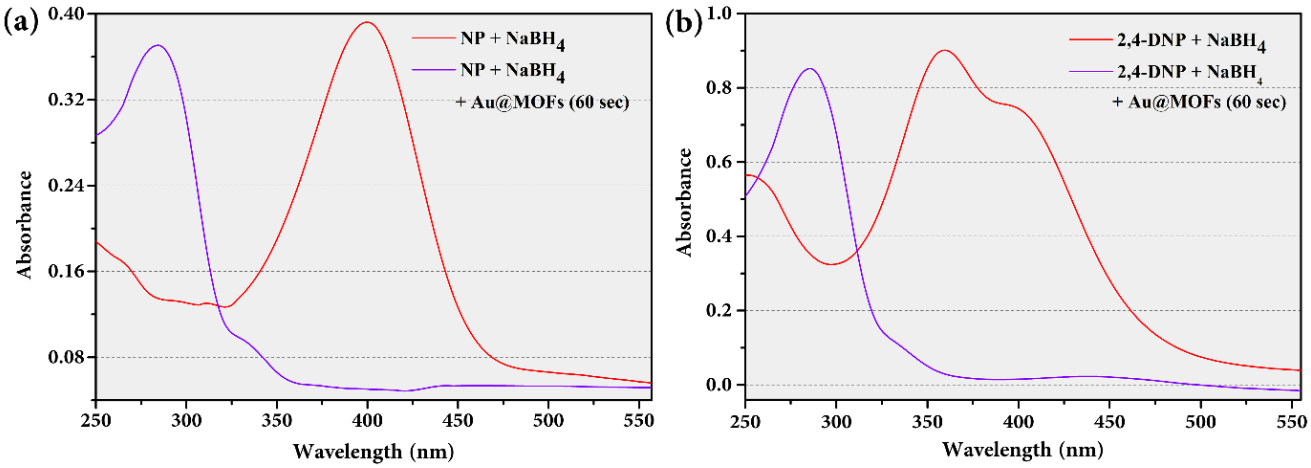

Fig. S13. *Absorption spectra of 4-NP and 2,4-DNP with $NaBH_4$ and after 60 sec addition of Au@MOFs. The appearance of new peak after addition of Au NPs indicated formation of reduced product.*

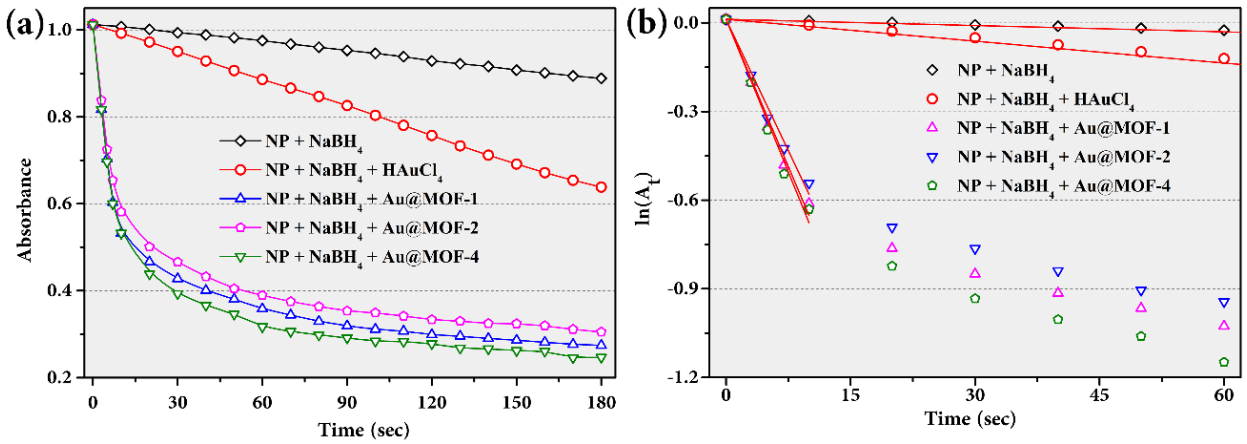

Fig. S14. *(a) Time dependent absorbance measurement of reduction process of 4-nitrophenol (NP) to 4-aminophenol with $NaBH_4$ in the presence of $HAuCl_4$, **Au@MOF-1**, **Au@MOF-2** and **Au@MOF-3**. (b) Corresponding ln(A_t) vs time (t) plots. The rate constants (k) were estimated by linear-fit (red lines) using equation 3.*

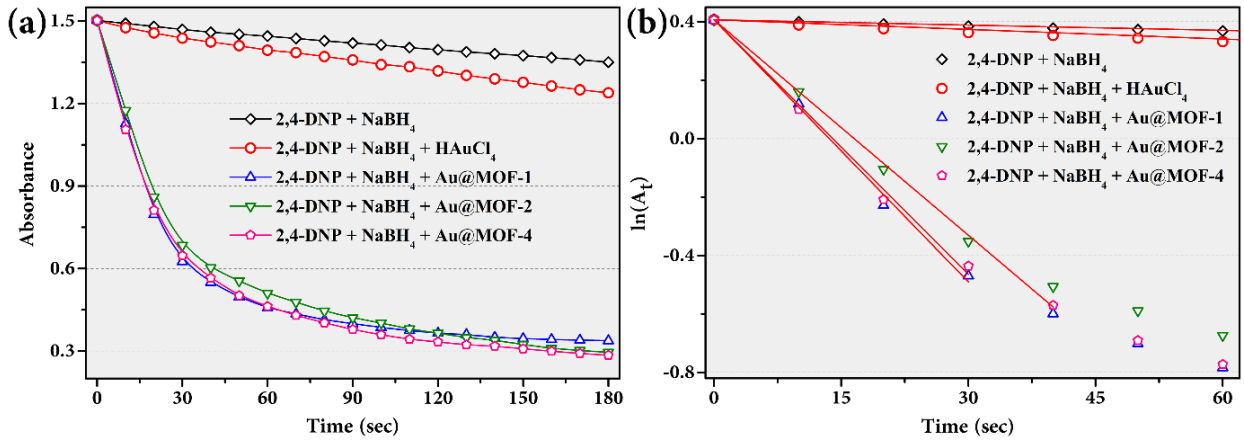

Fig. S15. *(a) Time dependent absorbance for the reduction of 2,4-DNP to 2,4-diaminophenol with $NaBH_4$ in the presence of $HAuCl_4$,* ***Au@MOF-1***, ***Au@MOF-2*** *and* ***Au@MOF-3****. (b) Corresponding ln(A_t) vs time (t) plots. The rate constants were estimated by linear-fit (red lines) using equation 3.*

Table S2. Rate constants for the Au@MOF catalyzed reduction of 4-NP and 2,4-DNP.

Analytes	Rate constants (sec^{-1})				
	Only $NaBH_4$	$HAuCl_4$	Au@MOF-1	Au@MOF-2	Au@MOF-3
4-NP	7.08×10^{-4}	2.47×10^{-3}	6.64×10^{-2}	5.92×10^{-2}	6.88×10^{-2}
2,4-DNP	6.05×10^{-4}	1.10×10^{-3}	2.99×10^{-2}	2.46×10^{-2}	2.90×10^{-2}

A comparison of catalytic activities between of these current Au@MOFs with other Au-supported porous substrates has been made, which is summarized in Table S3. All the rate constants were taken from respective references since all these catalytic reactions were carried out under almost similar experimental condition.

Table S3: Catalytic reductions of 4-nitrophenol by $NaBH_4$ in the presence of various supported Au nanoparticles.

Au@porous substrate	Rate constant (k/sec)	References
Au@NAP-Mg	7.6×10^{-3}	*Green Chem.*, 2012, **14**, 3164–3174
Au@Meso-HAP	4.4×10^{-3}	Green Chem., 2012, **14**, 3164–3174
Au@Meso-CeO_2	3.5×10^{-3}	*Green Chem.*, 2012, **14**, 3164–3174
Au@PAMAM G3	2.13×10^{-3}	*Langmuir*, 2003, **19**, 5517-5521
Au@SiO_2	4.6×10^{-4}	*Adv. Mater.*, 2008, **20**, 1523–1528
Au@CeO_2-NT	2.86×10^{-3}	*Applied Catalysis B: Environmental*, 2013, **132–133**, 107–115
Au@PPy-NTS	5.86×10^{-3}	*Applied Catalysis A: General*, 2012, **413–414**, 230–237
Au@MIL-100(Fe)	5.5×10^{-3}	*Chem. Commun.*, 2013, **49**, 1267-1269
Au@hm-ZrO_2	5.17×10^{-3}	*Small*, 2009, **5**, 361–365
Au@MOF-1	**6.64×10^{-2}**	**This work**
Au@MOF-2	**5.92×10^{-2}**	**This work**

Au@MOF-3	**6.88×10^{-2}**	**This work**

NAP-MgO = Nano Active™ Magnesium Oxide Plus, HAP = hydroxyapatite, PAMAM = poly(amidoamine) dendrimers, PPy-NTS = polypyrrole nanotubes, hm-ZrO_2 = hollow mesoporous-ZrO_2.

Stability of catalyst at higher temperature:

We have checked the stabilization of Au NPs by **MOF-3** with alkyne functionality by thermal annealing at 100 °C followed by TEM analysis. In typical annealing process, we sealed the sample in a glass tube under vacuum, subsequently it has been heated in a programmable oven for 3 h at 100 °C. After it cooled down to room temperature, the sample was prepared for TEM analysis. The TEM-BF images showed that the Au NPs remained mono-dispersed and particle size didn't change significantly compered to un-annealed sample (Fig. S16). Also, we performed TGA of **Au@MOF-3** up to 850°C and compared with that of activated **MOF-3** (Fig. S17). Interestingly, the stability of the **MOF-3** remained intact after loading of the Au NPs.

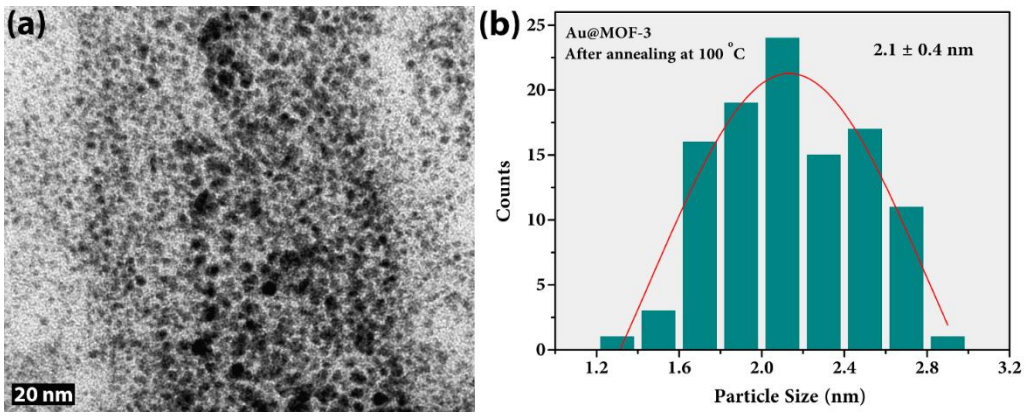

Fig. 16. (a) TEM-BF image of the **Au@MOF-3** after thermal annealing at 100 °C and (b) corresponding particle size distribution.

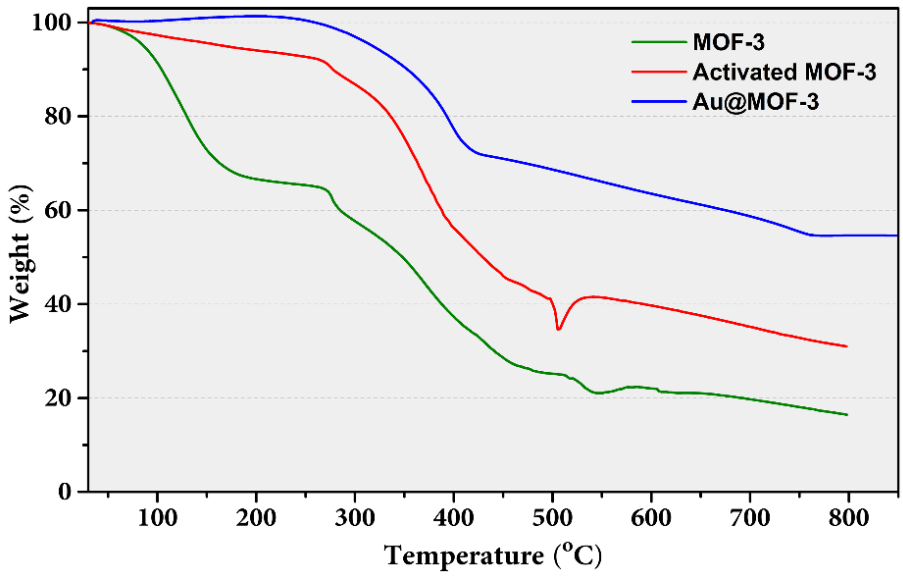

Fig. S17. *TGA of **Au@MOF-3** comparing with as synthesized **MOF-3** and activated **MOF-3**.*

Reusability Test of the catalyst:

The catalysts have been recovered by filtration and reused several times (5 times) without much loss of catalytic activity. The stability of the catalysts after reactions was established by TEM imaging (Fig. S18) and PXRD technique (Fig. S19) of the recovered catalysts. The non-aggregation of NPs clearly indicates the strong interaction between Au and MOFs through the functionalized ethynyl moiety.

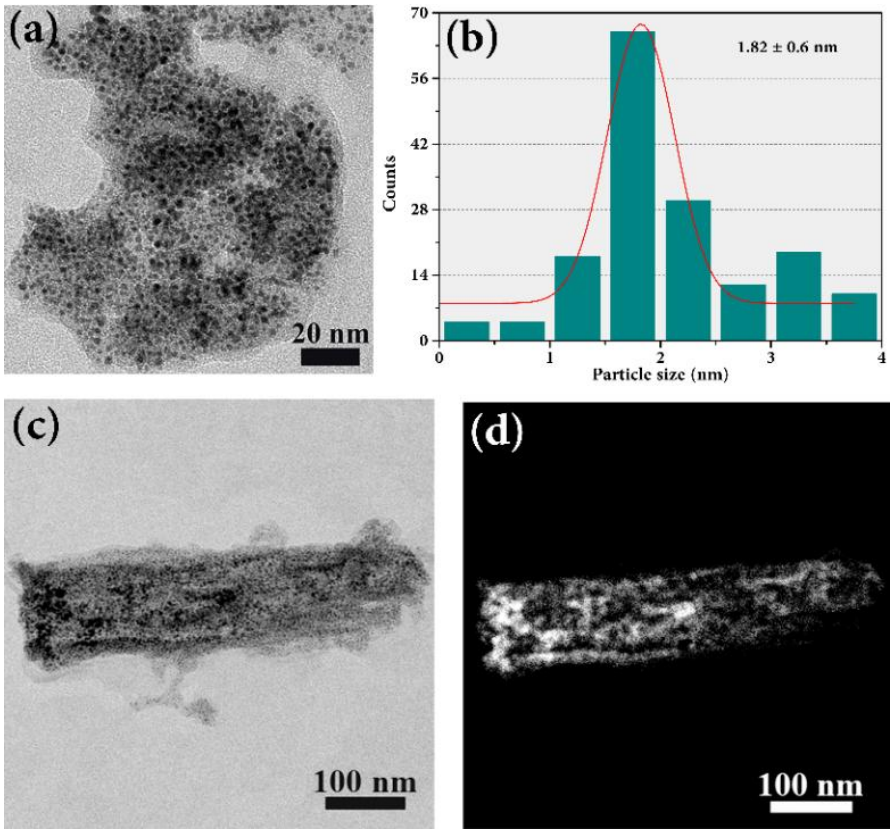

Fig. S18. *TEM images of recovered* ***Au@MOF-3*** *catalyst after five cycles. (a) Bright-field TEM image showing the Au NPs are homogeneously dispersed in* ***MOF-3****, (b) Corresponding Au NPs size distribution histogram and (c) Corresponding STEM bright field and (d) STEM-HAADF images.*

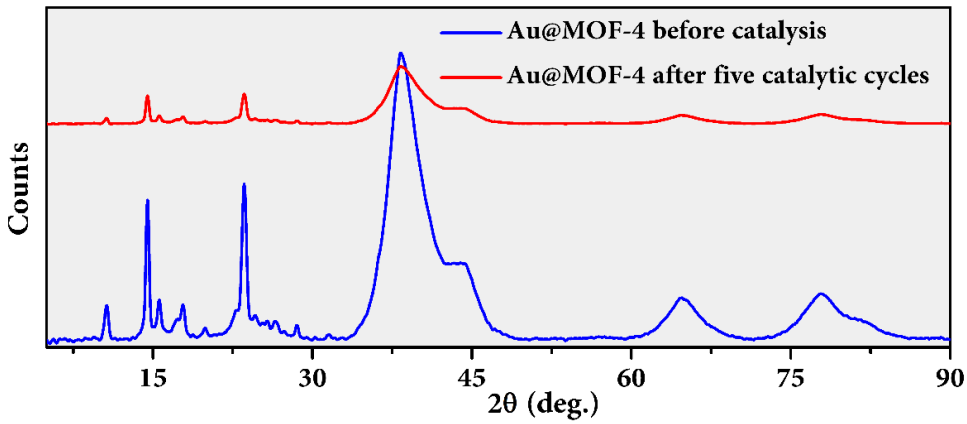

Fig. S19. *PXRD pattern of* ***Au@MOF-3*** *before and after catalytic cycles.*

4. Au@MOFs catalyzed reduction of aromatic nitro compounds in ethanol

To generalize the catalytic reduction to the other aromatic nitro compounds, several other analytes were chosen. Due to their insolubility in water the reductions were carried out in ethanol. To our surprise, with 2-3 equivalents of $NaBH_4$ and 5 mg (0.6 mol %) of Au@MOFs we could able to isolate corresponding azo compounds instead of expected amines. In a typical reaction method, aromatic nitro compounds (1 mmol), $NaBH_4$ (2 equivalents with respect to each nitro groups) and Au@MOFs were taken in a 10 mL scintillation vial. To the mixture 5 mL of ethanol was added with constant stirring. The catalytic reduction process was monitored by TLC. After 12 h the reaction mixture was completely dried and extracted with chloroform. Finally, slow evaporation of chloroform yielded highly crystalline orange materials. Subsequently, NMR and HRMS analysis confirmed the formation of azo products in contrast to the expected completely reduced product (amine). To understand whether the Au-NPs have any direct role in this coupling reaction, in a control experiment with only $NaBH_4$ does not produce either corresponding amine or azo.

4.1. Mechanistic investigations

It has been well known that the reduction of nitro group proceeds via intermediate nitroso compound, which subsequently reduced to the amine. However, the nitroso compounds are not quite stable in the presence of amine. Combination of both of them in solution readily produce coupling (azo) product. If the rate of the second reduction (nitroso to amine) is sufficiently faster than previous one (nitro to nitroso) then possibility of formation of azo compounds is extremely less. In the present case the mechanistic studies were carried out by time dependent ^{1}H-MNR spectroscopy wherein nitrobenzene (NB) has been used as model substrate in CD_3OD solution (Fig. 7). In a typical method, 0.5 mmol of NB (61.5 mg) was taken in an NMR tube. To that 0.5 mL of CD_3OD was added and subsequently ^{1}H-NMR spectra was recorded. $NaBH_4$ (1 mmol, 37.8 mg) and **Au@MOF-3** (2.5 mg) were added to the NMR tube successively. The NMR spectra of the solution was recorded during several time intervals (Fig. S20). The NMR studies indicated that the Au-NPs are involved in reactions, and initially produce nitroso compounds, which were further reduced to amine derivatives. However, the nitroso compounds are not quite stable in the presence of amine. Thus, combination of both of them in solution readily produced coupling (azo) product (Fig. S20).

Based on NMR studies, the plausible mechanism for **Au@MOF-3** catalyzed azobenzene derivative formation in alcohol is shown in Scheme S2. Initially, nitrobenzene reduced to nitrosobenzene (rate constant; k_1), which further reduced to aniline (k_2). In our case the rate of second reduction is slower ($k_1 > k_2$) which resulted in accumulation of nitroso intermediate. Thus, amine compound

produced in the reaction reacted further with nitroso intermediate which yielded azo product through water elimination (Scheme S2).

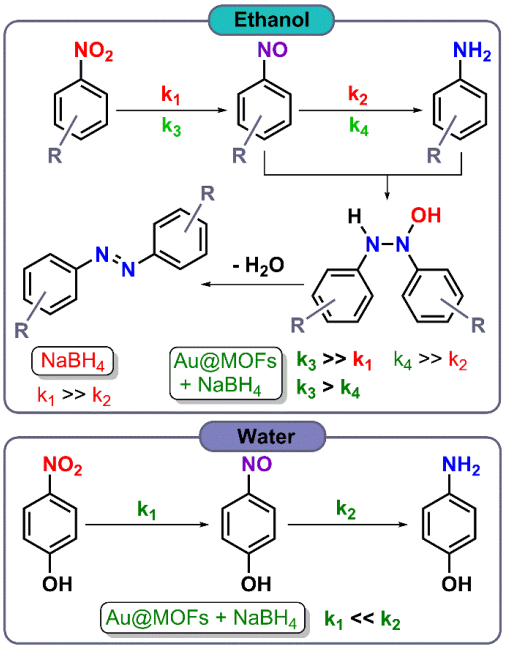

Scheme S2. Plausible way of formation of azo compounds by catalytic reduction of aromatic nitro derivatives by **Au@MOF-3** and $NaBH_4$ in ethanol and water.

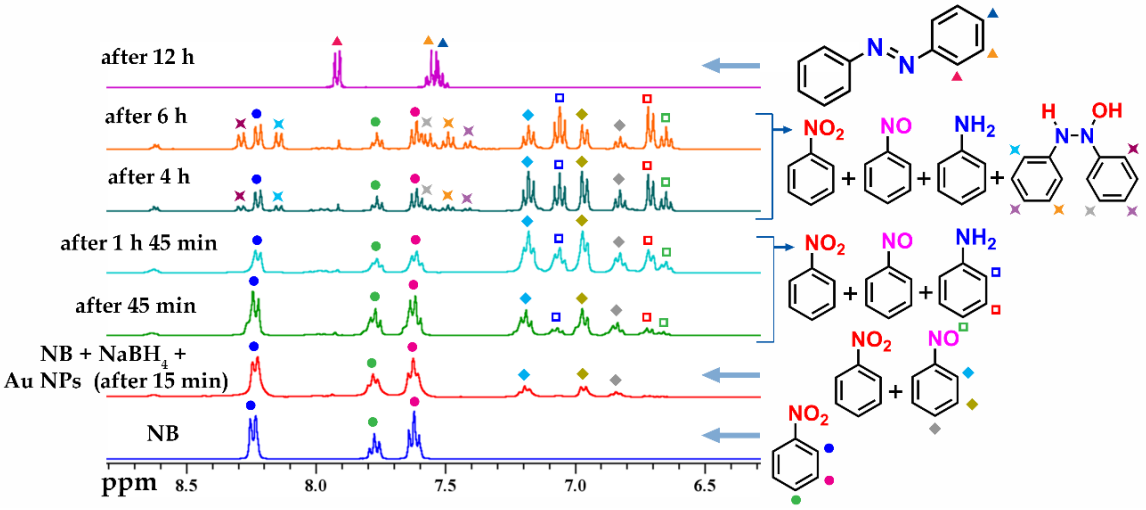

Fig. S20. *Mechanistic investigation of* ***Au@MOF-3*** *catalyzed reduction of NB in* CD_3OD *by time dependent* ^{1}*H-NMR spectroscopy.*

The control experiment was carried out in similar way instead only $NaBH_4$ was used. In the control reaction, the formation of nitroso is extremely slow (k_3) compared to **Au@MOF-3** catalyzed reaction and the second reduction to amine ($k_4 \approx 0$) is almost negligible as observed from the ^{1}H-NMR spectroscopy (Fig. S21). This control experiment showed that the direct involvement of the Au-NPs into the catalytic process. When the Au@MOFs catalytic reduction of 4-NP and 2,4-DNP were carried out in water the second reduction process is expected to be much faster ($k_1 << k_2$)

than the first reduction due to the higher dissociation of $NaBH_4$ in water compared to ethanol. Therefore, in water the reduced product is exclusively amine and also the conversion rate is extremely fast.

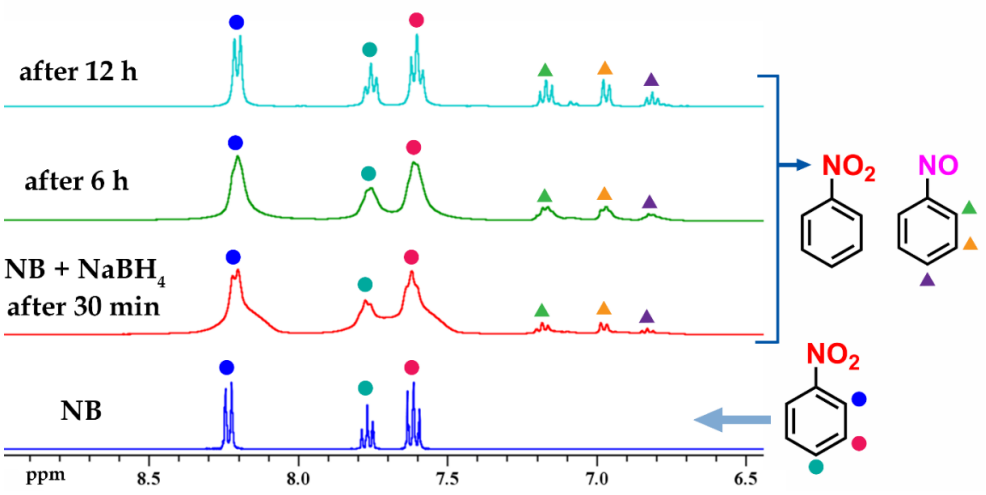

Fig. S21. *Control experiment with only $NaBH_4$. Time-dependent ^{1}H-NMR spectroscopy of NB in CD_3OD with only $NaBH_4$.*

5. Characterization of catalyzed products

All the azo products (as provided below) that were formed in ethanol were fully characterized by common NMR and high resolution mass spectroscopy.

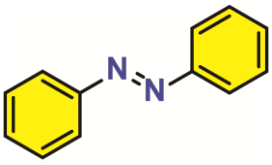

(E)-1,2-diphenyldiazene: ^{1}H NMR (400 MHz, CDCl3): δ (ppm) =7.94-7.92 (m, 4H), 7.54-7.48 (m, 6H). ^{13}C NMR (100 MHz, $CDCl_3$): δ (ppm) = 152.7, 131.0, 129.1, 122.9. HRMS: $[M+H]^+$ (183.0922), found: 183.0921.

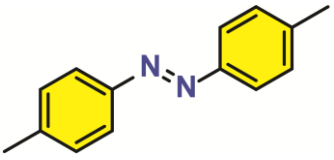

(E)-1,2-di-p-tolyldiazene: ^{1}H NMR (400 MHz, CDCl3): δ (ppm) =7.82-7.80 (d, 4H), 7.32-7.30 (d, 4H), 2.43 (s, 6H). ^{13}C NMR (100 MHz, $CDCl_3$): δ (ppm) = 21.71, 122.91, 129.91, 141.42, 150.99. HRMS: $[M+H]^+$ (211.1235), found: 211.1221.

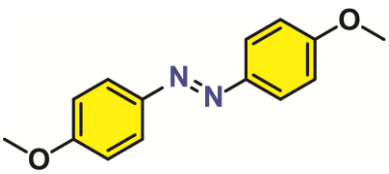

(E)-1,2-bis(4-methoxyphenyl)diazene: ^{1}H NMR (400 MHz, $CDCl_3$): δ (ppm) = 7.89-7.87 (d, 4H), 7.01-6.97 (d, 4H), 3.88 (s, 6H). ^{13}C NMR (100 MHz, $CDCl_3$): δ (ppm) = 161.98, 147.21, 124.47, 114.29, 55.81. HRMS: $[M+H]^+$ (243.1134), found: 243.1115.

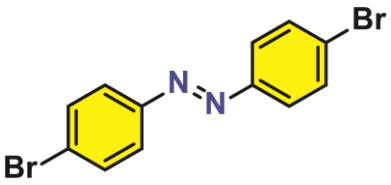

(E)-1,2-bis(4-bromophenyl)diazene: ^{1}H NMR (400 MHz, $CDCl_3$): δ (ppm) = 7.80-7.78 (d, 4H), 7.66-7.64 (d, 4H). ^{13}C NMR (100 MHz, $CDCl_3$): δ (ppm) = 132.57, 124.57. HRMS: $[M+H]^+$ (340.9107), found: 340.9146.

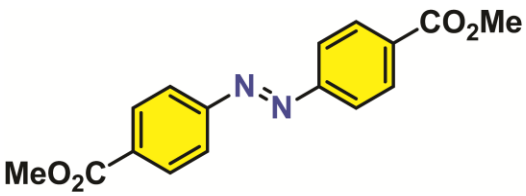

dimethyl 4,4'-(diazene-1,2-diyl)(E)-dibenzoate: ^{1}H NMR (400 MHz, $CDCl_3$): δ (ppm) = 8.21-8.19 (d, 4H), 7.99-7.97 (d, 4H). ^{13}C NMR (100 MHz, $CDCl_3$): δ (ppm) = 166.42, 154.95, 132.41, 130.68, 122.86, 52.44. HRMS: $[M+H]^+$ (299.1032), found: 299.1045.

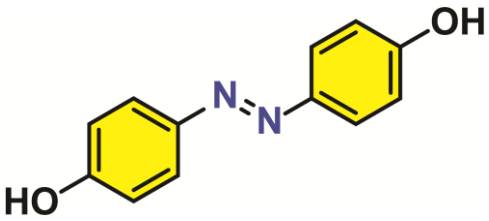

(E)-4,4'-(diazene-1,2-diyl)diphenol: ^{1}H NMR (400 MHz, CD_3OD): δ (ppm) = 7.97-7.95 (d, 4H), 6.49-6.47 (d, 4H). ^{13}C NMR (100 MHz, CD_3OD): δ (ppm) = 161.2, 147.4, 125.4, 116.5. HRMS: $[M+H]^+$ (215.0821), found: 215.0847.

(E)-1,2-di([1,1'-biphenyl]-3-yl)diazene: ^{1}H NMR (400 MHz, $CDCl_3$): δ (ppm) = 8.21 (s, 1H), 7.95-7.93 (d, 1H), 7.75-7.69 (m, 3H), 7.63-7.59 (t, 1H), 7.51-7.47 (m, 2H), 7.42-7.38 (m, 1H). ^{13}C NMR (100 MHz, $CDCl_3$): δ (ppm) = 153.59, 142.74, 140.86, 130.14, 129.98, 129.35, 128.18, 127.70, 122.15. HRMS: $[M+H]^+$ (335.1548), found: 335.1582.

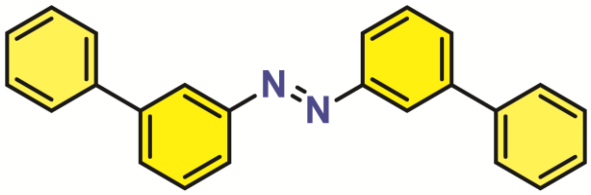

6. References

1. (a) Zhao, Y. L.; Dichtel, W. R.; Trabolsi, A.; Saha, S.; Aprahamian, I.; Stoddart, J. F. *J. Am. Chem. Soc.* **2008**, *130*, 11294. (b) Faust, T. B.; Bellini, V.; Candini, A.; Carretta, S.; Lorusso, G.; Allan, D. R.; Carthy, L.; Collison, D.; Docherty, R. J.; Kenyon, J.; Machin, J.; McInnes, E. J. L.; Muryn, C. A.; Nowell, H.; Pritchard, R. G.; Teat, S. J.; Timco, G. A.; Tuna, F.; Whitehead, G. F. S.; Wernsdorfer, W.; Affronte, M.; Winpenny, R. E. P. *Chem. Eur. J.* **2011**, *17*, 14020.

2. Gole, B.; Bar, A. K.; Mukherjee, P. S. *Chem. Eur. J.* **2014**, *20*, 2276.

3. SMART/SAINT; Bruker AXS, Inc.: Madison, WI, **2004**.

4. Sheldrick, G. M. SHELX-97; University of Göttingen: Göttingen, Germany, **1998**.

5. (a) Farrugia, L. J. *J. Appl. Crystallogr.* **1999**, *32*, 837. (b) Farrugia, L. J. WinGX, version 1.65.04; Department of Chemistry, University of Glasgow: Glasgow, Scotland, **2003**.

6. Sheldrick, G. M. SADABS; University of Göttingen: Göttingen, Germany, **1999**.